Research Article

Journal of Environmental Nanotechnology

Enterobacter cloacae Cell Lysate-mediated Biosynthesis of AgNPs: Physicochemical Characterization and Bactericidal Kinetics

Meyyarasan Kamalahasan[1], Kavitha Subramanian[2*], Venkatesa Prabhu Sundramurthy[3,4] and Saravanan Sundaram[5]

[1]Department of Microbiology, Karpagam Academy of Higher Education, Coimbatore, TN, India
[2]Department of Chemical Engineering, Hindusthan College of Engineering and Technology, Malumichampatti, Coimbatore, TN, India
[3]Department of Biotechnology, Faculty of Engineering, Karpagam Academy of Higher Education, Coimbatore, TN, India
[4]Centre for Natural Products and Functional Foods, Karpagam Academy of Higher Education, Coimbatore, TN, India
[5]Department of Chemical Engineering, V.S.B. Engineering College, Karur, TN, India
Received: 06.10.2025 Accepted: 20.12.2025 Published: 30.12.2025
*kavithajournal18@gmail.com

ABSTRACT

The biosynthesis of nanoparticles (NPs) offers a cost-effective and environmentally friendly approach. In the present study, lysate derived from *Enterobacter cloacae*, isolated from papaya fruit samples was utilized for the biological synthesis of silver nanoparticles (AgNPs). The biogenic AgNPs were characterized using X-ray diffraction (XRD), UV–visible spectroscopy, Fourier-transform infrared spectroscopy (FTIR), scanning electron microscopy (SEM), and X-ray Photoelectron Spectroscopy (XPS). The UV–visible spectra demonstrated characteristic bands corresponding to AgNPs, while XRD analysis confirmed their crystalline nature. The presence of capping proteins, which facilitate both the synthesis and stabilization of AgNPs was confirmed by FTIR. The SEM images revealed that the AgNPs were predominantly spherical, with their sizes ranging from 10 to 20 nm. The AgNPs were assessed for their antibacterial effectiveness against Gram-positive and Gram-negative bacteria by a modified disk diffusion technique. Remarkably, the AgNPs exhibited pronounced antibacterial activity against *Enterobacter cloacae* and *Pseudomonas aeruginosa*, highlighting their potential as effective antimicrobial agents.

Keywords: *Enterobacter cloacae;* Biosynthesis; Silver nanoparticles; Death kinetics; Antimicrobial activity.

1. INTRODUCTION

Nanotechnology has emerged as a rapidly advancing field that integrates principles from physics, chemistry, biology, and engineering to design and utilize materials at the nanoscale (Mohammed, 2025). Among the various nanomaterials investigated, silver nanoparticles (AgNPs) are gaining considerable interest due to their distinctive physicochemical characteristics, such as a high surface area-to-volume ratio, adjustable surface plasmon resonance, and robust biological activities (Meher *et al.* 2024). These features have enabled AgNPs to be applied extensively in medicine, food safety, environmental remediation, and antimicrobial formulations (Nawaz, *et al.* 2024).

Conventional chemical and physical methods of synthesis of AgNPs often involve hazardous reagents, high energy consumption, and generate toxic byproducts, raising concerns about sustainability and environmental implications. In this context, biological approaches, collectively known as “green synthesis” have been considered safe, cost-effective, and eco-friendly alternatives (Vidyasagar *et al.* 2023). Microorganisms, plant extracts, and biomolecules have been widely investigated as natural reducing and stabilizing agents for nanoparticle production. These biological systems provide inherent capping molecules, including proteins, polyphenols, and secondary metabolites, which not only facilitate the reduction of metal ions but also aid in improving nanoparticle stability and biocompatibility (Revathi *et al.* 2025; Hema *et al.* 2025).

Bacterial cell lysate offers several advantages for AgNP synthesis compared to plant extracts (Garg *et al.* 2020). The enzymatic mechanism in bacterial lysates enables rapid and more controlled reduction of silver ions, resulting in improved reproducibility and uniformity in nanoparticle size and shape. The biochemical composition of bacterial lysate is generally more consistent than that of plant extracts, which can vary with environmental and seasonal factors. This approach also allows easy scaling up and purification, making bacterial cell lysate a reliable platform for sustainable and efficient green nanoparticle synthesis (Durán *et al.* 2023).

Bacteria offer promising platforms for the biosynthesis of AgNPs due to their rapid growth, ease of handling, and metabolic diversity. Both intracellular and extracellular pathways have been reported for microbial nanoparticle synthesis, with extracellular approaches being advantageous for nanoparticle recovery and downstream processing. Among bacterial candidates, Enterobacter species are of significant interest because they produce a variety of cellular biomolecules such as enzymes, peptides, and reducing cofactors that can efficiently mediate nanoparticle formation (Rizwan *et al.* 2023). *Enterobacter cloacae*, a Gram-negative facultative anaerobe, is known for its adaptive metabolic potential and secretion of redox-active biomolecules, rendering it a suitable candidate for nanoparticle synthesis (Singh *et al.* 2025).

The current study focuses on the AgNPs synthesis using the cell lysate of *Enterobacter cloacae*. This approach aimed to elucidate the role of bacterial lysate in the reduction and stabilization of AgNPs and to evaluate the resulting nanoparticles in terms of their physicochemical characteristics and potential biological applications. By harnessing the intrinsic reducing capacity of bacterial lysates, this study contributes to the growing field of sustainable nanomaterial synthesis and underscores the potential of microbial resources in green nanotechnology.

2. MATERIALS AND METHODS

2.1 Isolation of Microorganism

Fresh papaya (*Carica papaya*) fruits were collected from a local market under aseptic conditions and transported to the laboratory in sterile containers. About 10 g of fruit tissue was mixed with 90 mL of sterile physiological saline (0.85% NaCl). Serial dilutions were made up to 10^{-6} mL, and 100 µL of each dilution was distributed on nutrient agar and MacConkey agar plates. The plates were incubated at 37 ± 2 ℃ for 24–48 hours. Distinct bacterial colonies with characteristic morphology were selected and streaked on fresh agar plates to obtain pure isolates.

2.2 Subculture Technique

Pure colonies were maintained by subculturing on nutrient agar slants under aseptic conditions. Subcultures were incubated at 37 ℃ for 24 hours and stored at 4 ℃ for short-term preservation. For long-term maintenance, glycerol stocks (20% v/v) were prepared and stored at –80 ℃.

2.3 Identification Using VITEK® 2 System

Presumptive isolates were subjected to biochemical identification using the VITEK® 2 Compact System (bioMérieux, France). A fresh colony from nutrient agar was suspended in sterile 0.45% NaCl solution to achieve a turbidity equivalent to 0.5 McFarland standard. The suspension was loaded into the VITEK® 2 GN identification card following the manufacturer's instructions. The card was automatically filled, sealed, and incubated in the VITEK® 2 system, where biochemical reactions were monitored kinetically. Identification was obtained through comparison with the VITEK® 2 database, and isolates showing high probability scores were confirmed as Enterobacter cloacae (Falgenhauer *et al.* 2021a).

2.4 Bacterial Cell Lysate Preparation

Isolated bacterial cultures were allowed to grown overnight at 37℃ to reach an optical density (OD_{600}) of 1.5–3.0. Cultures were centrifuged at 5,000 × g for 10 min to harvest the cells, and the supernatant was discarded. The cell pellet was resuspended in 5–10 volumes of sterile molecular-grade water. For enzymatic lysis, lysozyme was added and the suspension incubated at 37℃ for 30–60 min. Alternatively, mechanical disruption was performed using sonication with three 10 s bursts on ice, allowing 30 s intervals between each cycle. After lysis, cell debris has been separated by centrifugation at 10,000 × g for 10 min at 4℃, and the clear lysate was collected and stored at −80℃ for further use (Falgenhauer *et al.* 2021b).

2.5 Synthesis of AgNPs Using Bacterial Cell Lysate

AgNPs were synthesized by bioreduction of $AgNO_3$ using the prepared bacterial cell lysate as a reducing and stabilizing agent. Briefly, bacterial cell lysate was prepared as described previously and stored on ice. To synthesize AgNPs, an aqueous solution of $AgNO_3$ (1 mM) was mixed with the bacterial lysate at a typical volume ratio of 1:1 or optimized ratios. The solution mixture was incubated at 30±2 ℃ in the dark to prevent photoactivation of silver ions. Formation of AgNPs was monitored by the gradual color change of the solution from pale yellow to brown, indicating the reduction of Ag^+ ions to metallic silver nanoparticles. The reaction was allowed to proceed for 24–48 hours with gentle shaking to enhance homogeneous mixing. The synthesis progress was periodically checked by measuring UV-Visible absorbance in the range of 300–600 nm to detect the characteristic surface plasmon resonance (SPR) peak of AgNPs. After completion, the reaction mixture was centrifuged at 12,000 × g for 15 min to pellet the synthesized AgNPs. The pellet was washed multiple times with sterile distilled water to remove unreacted substances and bacterial residues. The purified AgNPs were then dried under vacuum and stored at 4℃ for further characterization and antimicrobial studies (Elbaghdady *et al.* 2018).

2.6 Characterization of AgNPs

The optical properties and formation of AgNPs were analyzed by measuring the UV–visible absorption spectra (300–600 nm) using a UV–Vis spectrophotometer. The crystalline nature and phase purity of the biosynthesized AgNPs were determined using X-ray diffraction (XRD) analysis. Dried AgNP powder was subjected to XRD scanning with Cu Kα radiation (wavelength λ = 1.5406 Å) over a 2θ range of 20° to 80°. The crystallite size was estimated using the Scherrer equation based on the prominent diffraction peak broadening. Fourier-Transform Infrared Spectroscopy (FTIR) was utilized to ascertain the functional groups of biomolecules responsible in the reduction and stabilization of AgNPs. To make samples, dried AgNPs were mixed with potassium bromide (KBr) and pressed into pellets. The acquired spectra from 4000 to 400 cm^{-1} showed typical absorption bands. The surface morphology and size distribution of the AgNPs were examined using Scanning Electron Microscopy (SEM). A sample of AgNP suspension was taken on a clean silicon wafer and dried under vacuum. High-resolution micrographs were acquired to observe the shape, size, and aggregation state of the synthesized nanoparticles. X-ray Photoelectron Spectroscopy (XPS) analysis was carried out to investigate the oxidation states of silver in the nanoparticles. Dried AgNPs samples were mounted on conductive carbon tape and analyzed under ultra-high vacuum conditions. High-resolution spectra were recorded, focusing on the Ag 3d core-level region to confirm metallic silver. Dynamic Light Scattering (DLS) measurements were conducted to determine the hydrodynamic diameter and size distribution of AgNPs in colloidal suspension. Samples were diluted appropriately and analyzed at room temperature. The technique measured the Brownian motion of particles to calculate their average size and polydispersity index, providing insights on nanoparticle stability and aggregation in suspension (Dhaka *et al.* 2023).

2.7 Antimicrobial Activity and Death Kinetics

The antimicrobial activity of the biosynthesized AgNPs was evaluated using the agar disk diffusion method against both Gram-positive and Gram-negative bacterial strains. The tested bacteria included Methicillin-resistant *Staphylococcus aureus* (MRSA), *Enterococcus faecalis* (Gram-positive), *Pseudomonas aeruginosa*, and *Enterobacter cloacae* (Gram-negative). Sterile Mueller-Hinton agar (MHA) plates were prepared and allowed to solidify. Each bacterial strain was cultured overnight in nutrient broth at 37°C and adjusted to approximately 0.5 McFarland turbidity standard (~1.5 × 10^8 CFU/mL). Using a sterile cotton swab, the bacterial suspension was evenly spread across the surface of the MHA plates to confirm uniform bacterial lawn formation. Sterile blank paper disks (5 mm diameter) were impregnated with 10 to 30 µL of the AgNPs sample solution and placed gently onto the inoculated agar surface. Dimethyl sulfoxide (DMSO) was used as the negative control, while tigecycline solution (1 mg/mL) was used as the positive control. All tests were performed in triplicate. The plates were incubated at 37°C for 24 hours. Following incubation, the zones of inhibition around each disk were measured in mm using a digital caliper. The diameter of the clear zone (including the disk diameter) indicated the antimicrobial efficacy of the AgNPs against the respective bacterial strain.

2.8 AgNPs Exposure and Cell Death Kinetics

Methicillin-resistant *Staphylococcus aureus* (for Gram-positive) and *Pseudomonas aeruginosa* (for Gram-negative) were used for kinetic bactericidal assays. Bacterial cultures were grown overnight in nutrient broth at 37°C and adjusted to approximately 0.5 McFarland standard (1.5 × 10^8 CFU/mL). For time-dependent bactericidal kinetics, AgNPs were freshly prepared in sterile distilled water and filter-sterilized. Bacterial suspensions were aliquoted and treated with various concentrations of AgNPs as follows: For *P. aeruginosa*, 100, 200, and 300 µg/mL of AgNPs and for MRSA, 500, 600, and 700 µg/mL of AgNPs were used. Control groups without AgNPs were included for each bacterial strain. About 10 mL of bacterial cultures were treated with the specified doses of AgNPs at 37°C while being agitated at 150 rpm. At selected time intervals (0, 50, 100, 150, 200, and 250 min), 100 µL samples were removed, serially diluted in sterile saline, and plated on nutrient agar to enumerate surviving colonies by the spread plate method. Plates were incubated at 37°C for 18–24 hours, after which colony-forming units (CFU) were enumerated and converted to log CFU/mL. Survival curves were plotted as log CFU *versus* incubation time for each condition to assess the bactericidal effect of AgNPs in a dose- and time-dependent manner. Each experiment was performed at least in triplicate, with results reported as means ± standard deviation.

3. RESULTS AND DISCUSSION

3.1 Identification of Gram-negative Bacteria Using the VITEK-2 System

The identification results obtained from the VITEK 2 system, highlighted its accuracy in identifying specific bacterial species and groups. The VITEK 2 system successfully identified *Enterobacter cloacae* isolates (BioNumber: 2627734553533010) with a 98% accuracy rate within 4.5 hours (Fig. 1).

The results indicate successful synthesis of AgNPs using *Enterobacter cloacae* cell lysate, as evidenced by a distinct color change from the pale bacterial lysate supernatant to a deep brown solution. The UV-visible spectroscopic analysis of the synthesized

nanoparticles revealed an SPR peak at 433 nm (Fig. 2). This SPR band is characteristic of AgNPs and signifies successful nanoparticle formation. The intensity and position of the peak suggest well-dispersed nanoparticles, which are typical in cell lysate-mediated biosynthesis processes. This data aligns closely with previously published work on *E. cloacae*-mediated AgNPs synthesis. Elbaghdady *et al*. (2018) reported that *E. cloacae* cell lysate-mediated synthesis produced AgNPs with a UV-Vis absorption maximum at 440 nm, correlating with the current result. Other studies on biosynthesized AgNPs generally find the SPR band in the 400–460 nm range, typical for nanoparticles produced by bacterial lysates (Solís-Sandí *et al.* 2023). Biofilm supernatant and other bacterial supernatants have been shown to induce a similar color change and produce peaks within 400–450 nm, reinforcing the reliability of UV-Vis as a monitoring technique for nanoparticle formation (Xia *et al.* 2023). Fig. 3(a) and (b) show the bacterial lysate supernatant and the appearance of solution after the synthesis of AgNPs using bacterial lysate supernatant.

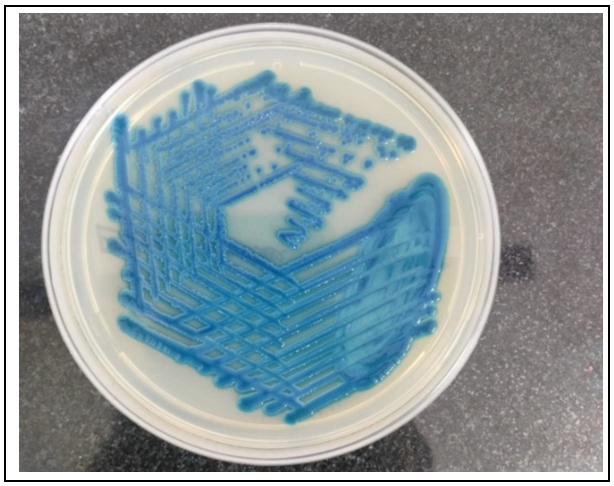


Fig. 1: Culture development of *E. cloacae* using the VITEK-2 system

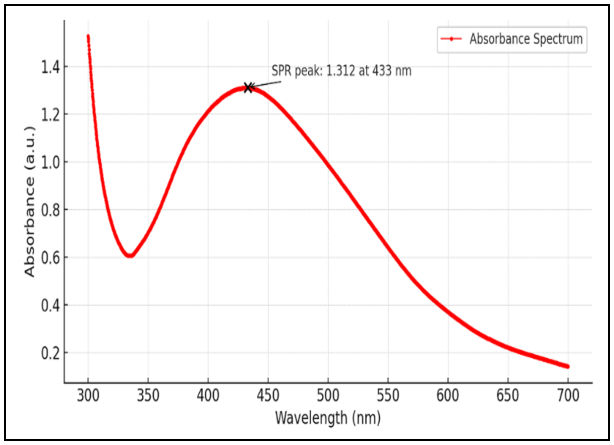


Fig. 2: UV-vis absorption spectrum confirming the formation of AgNPs

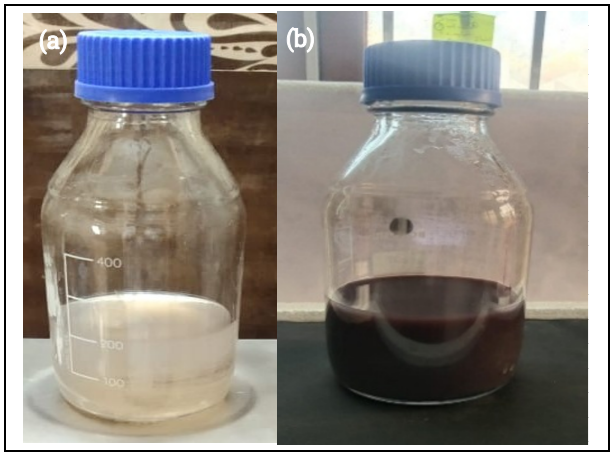


Fig. 3: (a) Bacterial lysate supernatant and (b) Appearance of solution after the synthesis of AgNPs

3.2 FTIR Spectroscopy Analysis

Fig. 4 revealed several characteristic absorption bands of AgNPs synthesized using *E. cloacae* lysate using FTIR spectroscopy analysis. Notable peaks were observed at 3485, 2926, 2360, 1726, 1640, 1558, 1444, 1417, 1367, 1316, 1266, 1018, 819, and 730 cm^{-1}. These peaks correspond to the vibrational frequencies of various functional groups present on the nanoparticle surface. The observed strong and broad peak at 3485 cm^{-1} can be attributed to O–H stretching (hydroxyl groups from alcohols or phenols) and N–H stretching vibrations (amines or amide groups), suggesting the presence of proteins or other biomolecules as capping agents on the surface of AgNPs. The peak at 2926 cm^{-1} is typically assigned to C–H stretching of aliphatic chains, while the peak near 2360 cm^{-1} may indicate the presence of carbon dioxide or carbonyl groups. The intense band at 1640 cm^{-1} likely corresponds to the amide I band of the peptide linkage (C=O stretching), confirming the involvement of proteinaceous substances from the lysate in both the reduction and stabilization of the nanoparticles (Huq, 2020).

Additional peaks around 1558 cm^{-1} (amide II, N–H bending and C–N stretching), 1444 – 1417 cm^{-1} (C–H bending, COO^- symmetric stretch), and 1367–1266 cm^{-1} (protein/polysaccharide groups) further support the participation of biological macromolecules from the lysate supernatant as reducing and capping agents during nanoparticle synthesis. The characteristic peak at 1018 cm^{-1} is attributable to C–O stretching vibrations, often present in alcohols, ethers, and polysaccharides. Peaks near 819 and 730 cm^{-1} suggest C–H bending and may imply polyol or aromatic ring structures (Singh and Mijakovic, 2022).

These findings are consistent with prior studies where FTIR spectra of biosynthesized AgNPs showed similar peaks indicative of proteins, peptides, and other biogenic molecules adsorbed onto the nanoparticle

surface. The presence of these functional groups confirms the dual role of microbial lysate, facilitating the reduction of Ag^+ ions to AgNPs and acting as stabilizing agents to prevent aggregation and confer colloidal stability. Similar conclusions were drawn by Elbaghdady *et al*. (2018), who noticed strong peaks for N–H, C=O, and C–N stretching, attributed to proteins and peptides capping AgNPs synthesized by *E. cloacae* lysate.

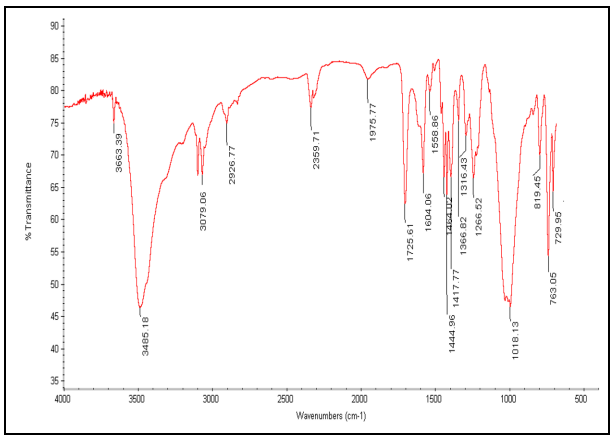


Fig. 4: FTIR spectrum of AgNPs synthesized using *Enterobacter cloacae* lysate

Fig. 5 illustrates the XRD pattern of synthesized AgNPs. The spectrum displays several prominent peaks in the 2θ range between 30° and 90°. Most intense peaks were observed at approximately 38°, 44°, 64°, and 77°, consistent with the (111), (200), (220), and (311) crystal planes of face-centered cubic (FCC) silver, as indexed by the JCPDS file No. 04-0783. Absence of extra peaks suggests highly pure and crystalline nature of the nanoparticles. The presence of strong diffraction peaks around 2θ = 38°, 44°, 64°, and 77° indicates that the biosynthesized AgNPs have an FCC crystalline structure. These peak positions closely match prior reports for biologically synthesized AgNPs using various bacteria and plant extracts, confirming successful nanoparticle formation and crystallinity. Theivasanthi and Alagar, (2011) and Gomes *et al.* (2025) described nearly identical XRD patterns for AgNPs, supporting that these peaks are reliable structural fingerprints for pure AgNPs.

Broadening of the diffraction peaks and high intensity suggest a small crystallite size and high degree of purity, common characteristics of biosynthesized AgNPs. Additional minor peaks at lower 2θ values can occasionally appear due to organic matter or residual biomolecules from the lysate used during synthesis, but they are generally much less intense and do not interfere significantly with AgNP assignments. The intense (111) reflection indicates preferential growth orientation, which has been associated with enhanced catalytic and antimicrobial activities in AgNPs. The crystalline nature and phase purity confirmed by XRD analysis, together with supporting literature, demonstrate that *E. cloacae* lysate provides an effective biogenic route for stable, high-quality AgNPs production. The observed pattern confirms that biosynthesized nanoparticles are structurally comparable to those produced chemically, with the benefit of environmentally friendly synthesis conditions.

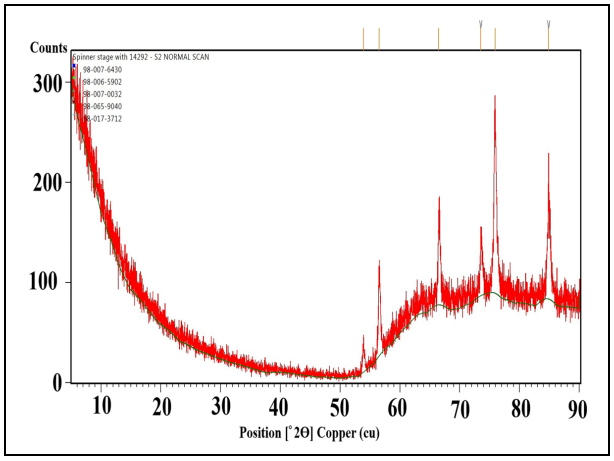


Fig. 5: XRD pattern of AgNPs synthesized using *Enterobacter cloacae* lysate

3.3 Scanning Electron Microscopy Studies

Fig. 6 shows the SEM images of AgNPs synthesized by the lysate of *E. cloacae* at magnifications of 10,000× and 50,000×, revealing their surface morphology and size distribution. The nanoparticles display predominantly spherical to near-spherical morphologies, with evidence of particle aggregation and dense packing throughout the sample. At higher magnification, the images indicate the presence of individual nanoparticles and small clusters, with most particles appearing below 50 nm in diameter, while larger aggregates are also visible (Tavakkoli *et al.* 2022). The observed spherical morphology and nanoscale size range are characteristic features of biologically synthesized AgNPs, consistent with previous studies using *E. cloacae* and similar bacterial systems. The aggregation seen in the images is typical for AgNPs synthesized in biological matrices, where biomolecules present in the lysate may act as both capping and stabilizing agents but can also promote some degree of agglomeration, particularly upon drying for SEM preparation (Badar *et al.* 2020). Comparable works have demonstrated that biologically and green-synthesized AgNPs exhibit similar shapes and size distributions, with a tendency toward small, globular, and monodispersed particles. Particle sizes can be somewhat larger in SEM due to aggregation and the effects of sample preparation. The observed morphology supports efficient nucleation and stabilization mediated by proteins and other biomolecules released by *E. cloacae*, as cited in both this and previous reports (Thomas *et al.* 2014).

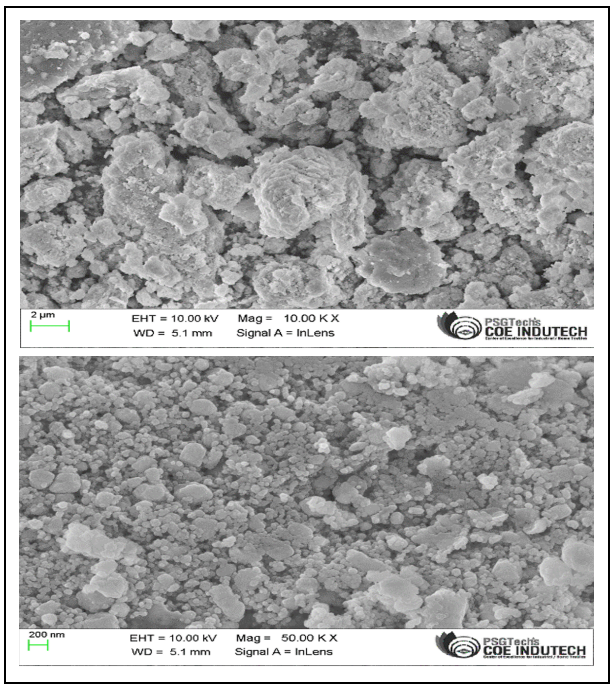


Fig. 6: SEM micrographs of synthesized AgNPs at magnifications of 10,000× and 50,000×

Fig. 7 displays the EDX spectrum of the synthesized AgNPs with prominent peaks corresponding to elemental Ag, in addition to peaks for O, C, and Cl. The major peaks for silver were observed at around 3 keV, which are characteristic of metallic silver and thereby confirming the successful AgNPs synthesis. The additional peaks for O, C, and Cl indicate the presence of biomolecules and possible residual ions associated with the bacterial lysate (Alam, 2022). The strong, well-defined Ag peaks at approximately 3 keV are a definitive indicator of AgNPs and are routinely observed in the EDX spectra of biosynthesized AgNPs across various biological systems. The carbon and oxygen peaks arise from capping and stabilizing biomolecules derived from the lysate, commonly including proteins, polysaccharides, or other organic compounds that coat the nanoparticles during synthesis. Peaks for chlorine are frequently seen in biosynthetic protocols and typically result from buffer salts or biomolecular residues (Jafar and Athbi, 2024).

Previous studies on green and bacterial synthesis consistently report EDX profiles with silver as the major constituent (often 72% by weight), alongside lighter elements such as O, C, and Cl, confirming both the elemental purity and the biological origin of the capping agents. These surface biomolecules enhance nanoparticle stability, inhibit agglomeration, and may also impart additional functional properties of biological activity (Rashidi *et al.* 2024).

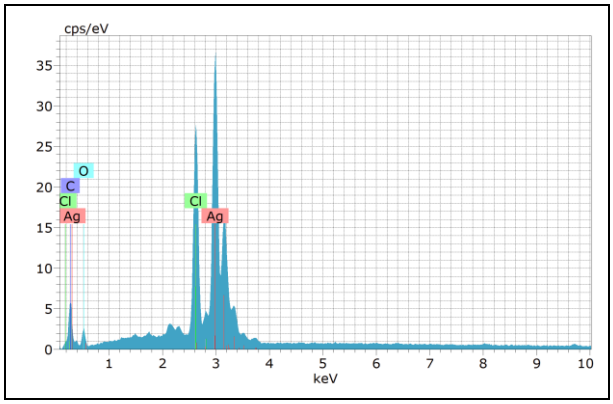


Fig. 7: EDX spectrum of the synthesized AgNPs

3.4 Anti-bacterial Activity

Fig. 8 shows the results obtained from antibacterial activity test using AgNPs synthesized by disk diffusion method. The disk diffusion assay demonstrates clear zones of inhibition around AgNP-impregnated disks at different concentrations (10–30 µg/disc) against all tested bacterial strains. The positive control (P.C) consistently shows a prominent inhibitory zone for each organism, confirming assay validity, while the negative control (N.C) shows no inhibition. In all cases, increased AgNPs concentration correlates with an increased zone of inhibition, with maximal effects observed at 25 and 30 µg concentrations. The observed antibacterial effectiveness of AgNPs synthesized by *E. cloacae* lysate against a panel of Gram-positive (MRSA and *E. faecalis*) and Gram-negative (*E. cloacae* and *P. aeruginosa*) bacteria aligns with broad-spectrum activity reported in the literature (Franci *et al.* 2015). Similarly, results from Elbaghdady *et al.* (2018) and Bruna *et al.* (2021) confirm that biosynthesized AgNPs can inhibit both resistant and non-resistant clinical pathogens, often at lower concentrations than conventional antibiotics. The larger inhibition zones at greater AgNP concentrations (25–30 µg/disc) are consistent with dose-dependent antimicrobial effects described in several studies, with Gram-negative bacteria (*E. cloacae*, *P. aeruginosa*) typically displaying similar or slightly higher susceptibility compared to Gram-positive counterparts.

Mechanistically, AgNPs exert their bactericidal action by disrupting bacterial membranes, generating reactive oxygen species, and interfering with cellular components, regardless of cell wall architecture, though Gram-negative organisms can sometimes show enhanced sensitivity due to thinner peptidoglycan layers. This pan-bacterial activity, including against multidrug-resistant strains like MRSA, reinforces the potential of

biosynthesized AgNPs as effective antimicrobial agents (More *et al.* 2023a).

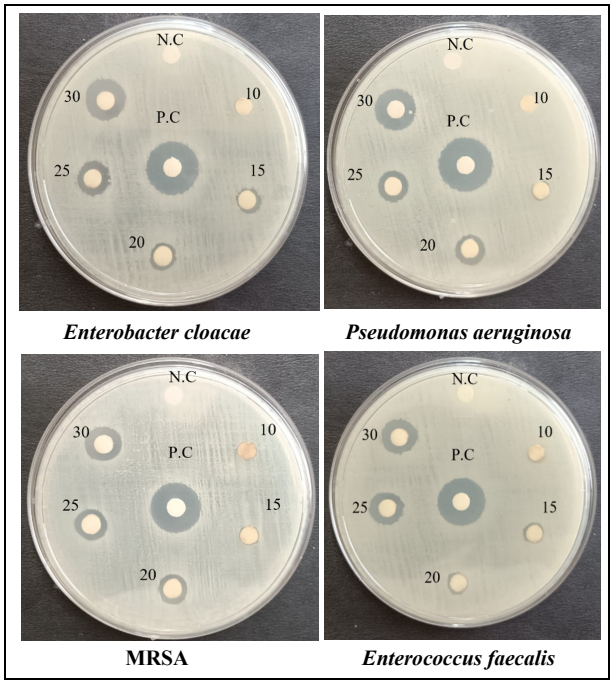


Fig. 8: Antibacterial activity of AgNPs synthesized by disk diffusion method. NC: negative control - DMSO; PC: positive control - tigecycline (1 mg/mL); sample volumes applied: 10 µL and 30 µL

The XPS analysis (Fig. 9) confirms the successful reduction of silver ions to their elemental metallic state (Ag^0), a key indicator of complete nanoparticle synthesis. This is further evidenced by the presence of Ag 3d5/2 and Ag 3d3/2 peaks at their characteristic binding energies, a widely reported feature for biosynthesized AgNPs (Petkar *et al.* 2022 and Balashanmugam *et al.* 2016). The high intensity and sharpness of these peaks indicate high surface purity of silver, with minimal contribution from oxidized states. Fig. 10 shows the DLS analysis graph with a narrow particle size distribution. It shows a peak in the <50 nm range, which is consistent with green and bacterial biosynthesis methods where proteins and biomolecules in the lysate regulate nucleation and growth (Ghasemi *et al.* 2024). The size range matches even smaller than AgNPs produced by chemical routes, supporting enhanced antibacterial activity due to increased surface area. As shown in Fig. 11, the zeta potential value of −42.8 mV is considerably more negative than the stability threshold of ±30 mV, suggesting that the AgNPs possess excellent stability and will resist aggregation in suspension. Previous reports highlight that strongly negative zeta potential, facilitated by capping with negatively charged biomolecules, is key for long-term colloidal stability and bio-interaction (Răut *et al.* 2024).

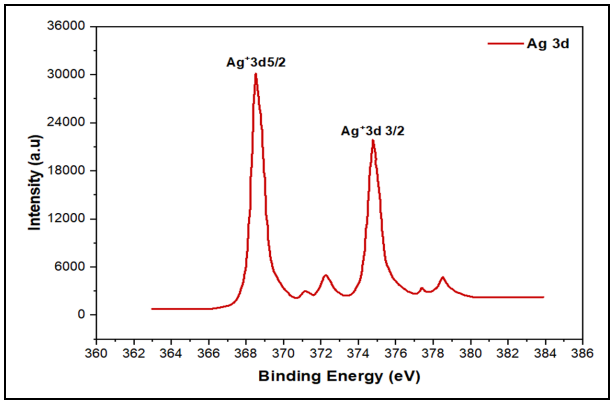


Fig. 9: XPS spectrum of metallic silver nanoparticles

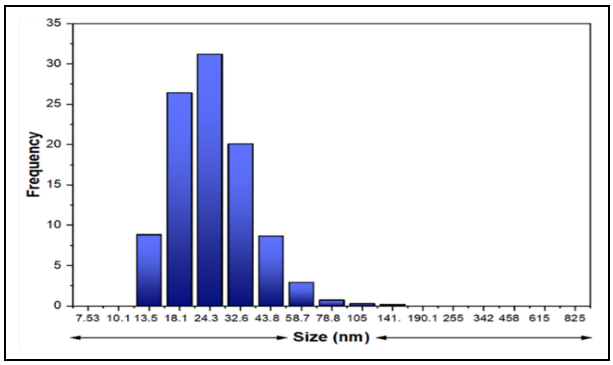


Fig. 10: DLS analysis for size distribution of nanoparticles

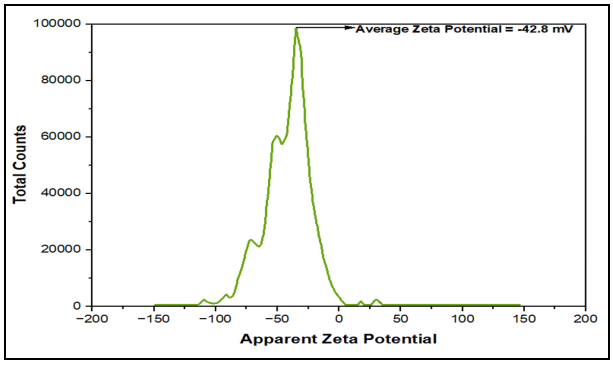


Fig. 11: Analysis of zeta potential measurement on AgNPs

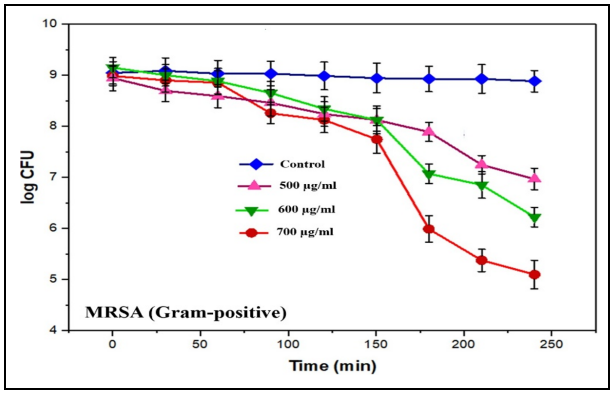


Fig. 12: Kinetic bactericidal assay of AgNPs against MRSA (Gram-positive)

3.5 The kinetic Bactericidal Assays Using AgNPs

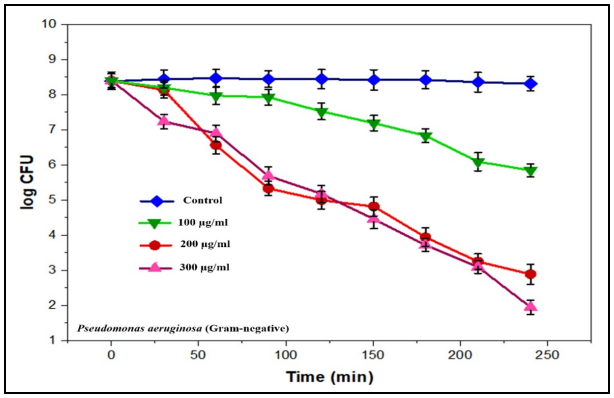


Fig. 13: Kinetic bactericidal assay of AgNPs against *Pseudomonas aeruginosa* (gram-negative)

Time-kill kinetic assays were carried out by exposing MRSA and *Pseudomonas aeruginosa* to varying concentrations of AgNPs (Fig. 12 and 13), monitoring changes in viable cell counts (log CFU/mL) over a 250-min incubation period. For MRSA, treatment with 500, 600, and 700 µg/mL AgNPs resulted in a clear, concentration-dependent reduction in bacterial viability. The highest concentration (700 µg/mL) achieved a rapid and pronounced bactericidal effect, reducing MRSA cell counts by over 4 log units within 250 minutes, while lower concentrations showed less pronounced but significant declines. For *P. aeruginosa*, lower AgNP concentrations (100, 200, and 300 µg/mL) were used, and the results similarly displayed a sharp, dose-dependent decrease in viable cells. The greatest reduction was observed at 300 µg/mL, where viable counts dropped below detectable limits within the incubation window. In all experiments, control groups without AgNPs showed minimal loss of viability, confirming the specificity of the AgNP-induced bactericidal effect. These kinetic bactericidal results demonstrate that biosynthesized AgNPs exhibit rapid, potent, and concentration-dependent antimicrobial action against both Gram-positive (MRSA) and Gram-negative (*P. aeruginosa*) pathogens. The observed difference in required concentrations higher doses for MRSA compared to P. *aeruginosa* may be attributed to the thicker peptidoglycan layer in Gram-positive bacteria, which can hinder nanoparticle penetration and antimicrobial efficacy. The rapid decline in bacterial viability, especially at higher AgNP concentrations, is consistent with published studies reporting that AgNPs disrupt bacterial membranes, induce oxidative stress, and damage DNA, leading to swift and irreversible cell death (More *et al.* 2023b). These findings support the broad-spectrum utility of AgNPs, including against drug-resistant strains like MRSA, and highlight their potential as alternative or adjunctive antimicrobial agents (Dakal *et al.* 2016). The kinetic assay data further validate that the biosynthetic route utilizing *E. cloacae* lysate yields AgNPs capable of overcoming key bacterial defense mechanisms, aligning with current literature on the time- and dose-dependent bactericidal action of nanomaterials derived *via* green synthesis.

4. CONCLUSION

This study demonstrates the successful biosynthesis of AgNPs using the cell lysate of *Enterobacter cloacae*, providing a sustainable and environmentally friendly alternative to conventional chemical methods. The AgNPs produced were well characterized and found to be predominantly spherical, crystalline, and within the nanoscale range, with strong evidence of bio-organic capping as revealed by FTIR, SEM, UV-Vis, XRD, XPS, DLS, and zeta potential analyses. Antibacterial assays showed that these biogenic AgNPs exhibit potent activity against both Gram-positive and Gram-negative pathogens, with efficacy confirmed in both disk diffusion and kinetic bactericidal assays. Notably, time- and dose-dependent killing was demonstrated, with rapid reductions in bacterial viability at higher nanoparticle concentrations. Further research, especially regarding biocompatibility and environmental impact, is essential before clinical or large-scale implementation can be considered.

CONFLICTS OF INTEREST

The authors declare that there is no conflict of interest.

FUNDING

Not Applicable

CONTRIBUTION STATEMENT FOR RESEARCH AND MANUSCRIPT

Meyyarasan Kamalahasan: Writing original draft, Conceptualization, Methodology, and Data curation; Kavitha Subramanian: Investigation, supervision and Validation. Venkatesa Prabhu Sundramurthy: Editing draft, Project administration, Saravanan Sundaram: Visualization Formal analysis, and Data curation.

COPYRIGHT

This article is an open access article distributed under the terms and conditions of the Creative Commons Attribution (CC-BY) license (http://creativecommons.org/licenses/by/4.0/).

REFERENCES

Alam, M., Analyses of biosynthesized silver nanoparticles produced from strawberry fruit pomace extracts in terms of biocompatibility, cytotoxicity, antioxidant ability, photodegradation, and in-silico studies, *J. King Saud Univ. – Sci.,* 34(8), 102327 (2022). https://doi.org/10.1016/j.jksus.2022.102327

Badar, W. and Khan, M. A. U., Analytical study of biosynthesised silver nanoparticles against multi-drug resistant biofilm-forming pathogens, *IET Nanobiotechnology*, 14(4), 331–340 (2020). https://doi.org/10.1049/iet-nbt.2019.0287

Balashanmugam, P., Balakumaran, M. D., Murugan, R., Dhanapal, K. and Kalaichelvan, P. T., Phytogenic synthesis of silver nanoparticles, optimization and evaluation of in vitro antifungal activity against human and plant pathogens, *Microbiol. Res.,* 192, 52–64 (2016). https://doi.org/10.1016/j.micres.2016.06.004

Bruna, T., Maldonado-Bravo, F., Jara, P. and Caro, N., Silver nanoparticles and their antibacterial applications, *Int. J. Mol. Sci.,* 22(13), 7202 (2021). https://doi.org/10.3390/ijms22137202

Dakal, T. C., Kumar, A., Majumdar, R. S. and Yadav, V., Mechanistic basis of antimicrobial actions of silver nanoparticles, *Front. Microbiol.,* 7, 1831 (2016). https://doi.org/10.3389/fmicb.2016.01831

Dhaka, A., Mali, S. C., Sharma, S. and Trivedi, R., A review on biological synthesis of silver nanoparticles and their potential applications, *Results Chem.,* 6, 101108 (2023). https://doi.org/10.1016/j.rechem.2023.101108

Durán, N., Fávaro, W. J., Alborés, S., da Costa, T. S. and Tasic, L., Biogenic silver nanoparticles capped with proteins: Timed knowledge and perspectives, *J. Braz. Chem. Soc.,* 34(7), 897–905 (2023). https://doi.org/10.21577/0103-5053.20230062

Elbaghdady, K., El-Shatoury, E., Abdallah, O. and Khalil, M., Biogenic production of silver nanoparticles by *Enterobacter cloacae* Ism26, *Turkish J. Biol.,* 42(4), 319–328 (2018). https://doi.org/10.3906/biy-1801-53

Falgenhauer, E., von Schönberg, S., Meng, C., Mückl, A., Vogele, K., Emslander, Q., Ludwig, C. and Simmel, F. C., Evaluation of an *E. coli* cell extract prepared by lysozyme-assisted sonication via gene expression, phage assembly and proteomics, *ChemBioChem,* 22(18), 2805–2813 (2021). https://doi.org/10.1002/cbic.202100257

Falgenhauer, E., von Schönberg, S., Meng, C., Mückl, A., Vogele, K., Emslander, Q., Ludwig, C. and Simmel, F. C., Evaluation of an *E. coli* cell extract prepared by lysozyme-assisted sonication via gene expression, phage assembly and proteomics, *ChemBioChem,* 22(18), 2805–2813 (2021). https://doi.org/10.1002/cbic.202100257

Franci, G., Falanga, A., Galdiero, S., Palomba, L., Rai, M., Morelli, G. and Galdiero, M., Silver nanoparticles as potential antibacterial agents, *Mol.,* 20(5), 8856–8874 (2015). https://doi.org/10.3390/molecules20058856

Garg, D., Sarkar, A., Chand, P., Bansal, P., Gola, D., Sharma, S., Khantwal, S., Surabhi, Mehrotra, R., Chauhan, N. and Bharti, R. K., Synthesis of silver nanoparticles utilizing various biological systems: Mechanisms and applications — a review, *Prog. Biomater.,* 9(3), 81–95 (2020). https://doi.org/10.1007/s40204-020-00135-2

Ghasemi, S., Dabirian, S., Kariminejad, F., Koohi, D. E., Nemattalab, M., Majidimoghadam, S., Zamani, E. and Yousefbeyk, F., Process optimization for green synthesis of silver nanoparticles using *Rubus discolor* leaves extract and its biological activities against multi-drug resistant bacteria and cancer cells, *Sci. Rep., 14*, 4130 (2024). https://doi.org/10.1038/s41598-024-54702-9

Gomes, B., Murucci, M. D., de Souza, W., Dal-Cheri, K. B.,Resend, A., Yoshihara, N., Geaquinto, L., Granjeiro, J. M., Sant'Anna, C. and Boldrini, L., Defining acceptance criteria for silver nanoparticles: correlating synthesis quality with biological outcomes in an in vitro lung cancer model, *Nano Trends,* 9, 100090 (2025). https://doi.org/10.1016/j.nwnano.2025.100090

Hema, K., Anishia, S. R., Rajeswari, S., Padmavathy, V., Sujatha, S. and Thiyagu, M., Green synthesis and multifunctional applications of *Moringa oleifera*-enhanced TiO_2 nanocomposites, *J. Environ. Nanotechnol.,* 14(1), 7–17 (2025). https://doi.org/10.13074/jent.2025.03.2511225

Huq, M. A., Green Synthesis of Silver Nanoparticles Using Pseudoduganella eburnea MAHUQ-39 and Their Antimicrobial Mechanisms Investigation against Drug Resistant Human Pathogens, *Int. J. Mol. Sci.,* 21(4), 1510 (2020). https://doi.org/10.3390/ijms21041510

Jafar, Z. N. and Athbi, A. M., Biosynthesis of Silver Nanoparticles Using Ethanolic Extract of the Marine Alga Enteromorpha intestinalis and Evaluation of their Antibacterial Activity, *Egypt. J. Aquat. Biol. Fish.,* 28(2), 735–756 (2024). https://doi.org/10.21608/ejabf.2024.350083

Meher, A., Tandi, A., Moharana, S., Chakroborty, S., Mohapatra, S. S., Mondal, A., Dey, S. and Chandra, P., Silver nanoparticle for biomedical applications: A review, *Hybrid Adv.,* 6(2), 100184 (2024). https://doi.org/10.1016/j.hybadv.2024.100184

Mohammed, Z. S., Role of nanotechnology in sustainable energy systems, *J. Environ. Nanotechnol.,* 14(2), 82–95 (2025). https://doi.org/10.13074/jent.2025.06.2511381

More, P. R., Pandit, S., Di Lisio, F., Franci, G., Mijakovic, I. and Galdiero, M., Silver nanoparticles: Bactericidal and mechanistic approach against drug resistant pathogens, *Microorg.,* 11(2), 369 (2023). https://doi.org/10.3390/microorganisms11020369

Nawaz, N., Ahmad, I. and Hussain, I., Biophysical characterization and biological applications of silver nanoparticles derived from *Ficus carica*, *J. Popul. Ther. Clin. Pharmacol.,* 31(5), 656–667 (2024). https://doi.org/10.53555/jptcp.v31i5.6216

Rashidi, M. A., Falahi, S., Dehghan, F. S., Ebrahimzadeh, H., Ghaneialvar, H. and Zendehdel, R., Green synthesis of silver nanoparticles by *Smyrnium cordifolium* plant and its application for colorimetric detection of ammonia, *Sci. Rep.,* 14, 24161 (2024). https://doi.org/10.1038/s41598-024-73010-w

Răut, I., Constantin, M., Șuică-Bunghez, R., Firincă, C., Alexandrescu, E., Gîfu, I. C., Doni, M., Zamfir, L. G., Gurban, A. M. and Jecu, L., Extracellular biosynthesis, characterization and antimicrobial activity of silver nanoparticles synthesized by filamentous fungi, *J. Fungi,* 10(11), 798 (2024). https://doi.org/10.3390/jof10110798

Revathi, A., Kalaivani, K., Sriram, K. and Venkatagiri, M., Sustainable synthesis of iron oxide using Plumeria alba flowers: Enhanced dye removal and its antimicrobial activity, *J. Environ. Nanotechnol*., 14(3), 29–38 (2025). https://doi.org/10.13074/jent.2025.09.2511374

Rizwan, M., Faisal, S., Tariq, M. H., Zafar, S., Khan, A. and Ahmad, F., Enterobacter hormaechei-driven novel biosynthesis of tin oxide nanoparticles and evaluation of their anti-aging, cytotoxic, and enzyme inhibition potential, *ACS Omega,* 8(30), 27439–27449 (2023). https://doi.org/10.1021/acsomega.3c02932

Singh, P. and Mijakovic, I., Strong Antimicrobial Activity of Silver Nanoparticles Obtained by the Green Synthesis in *Viridibacillus* sp. Extracts, *Front. Microbiol.,* 13, 820048 (2022). https://doi.org/10.3389/fmicb.2022.820048

Singh, S., Singh, A. K., Singh, S. K., Yadav, V. B., Kumar, A. and Nath, G., Current update on the antibiotic resistance profile and the emergence of colistin resistance in *Enterobacter* isolates from hospital-acquired infections, *Microbe,* 8, 100432 (2025). https://doi.org/10.1016/j.microb.2025.100432

Solís-Sandí, I., Cordero-Fuentes, S., Pereira-Reyes, R., Vega-Baudrit, J. R., Batista-Menezes, D. and Montes de Oca-Vásquez, G., Optimization of the biosynthesis of silver nanoparticles using bacterial extracts and their antimicrobial potential, *Biotechnol. Rep.*, 40, e00816 (2023). https://doi.org/10.1016/j.btre.2023.e00816

Theivasanthi, T. and Alagar, M., Electrolytic Synthesis and Characterizations of Silver Nanopowder, arXiv:1111.0260; (2011) https://doi.org/10.48550/arXiv.1111.0260

Thomas, R., Janardhanan, A., Varghese, R. T., Soniya, E. V., Mathew, J. and Radhakrishnan, E. K., Antibacterial properties of silver nanoparticles synthesized by marine *Ochrobactrum* sp, *Braz. J. Microbiol.,* 45(4), 1221–1227 (2014). https://doi.org/10.1590/S1517-83822014000400012

Vidyasagar, N., Patel, R. R., Singh, S. K. and Singh, M., Green synthesis of silver nanoparticles: Methods, biological applications, delivery and toxicity, *Mater. Adv.,* *4*(8), 1831–1849 (2023). https://doi.org/10.1039/D2MA01105K

Xia, F., Tao, X., Wang, H., Shui, J., Min, C., Xia, Y., Li, J., Tang, M., Liu, Z., Hu, Y., Luo, H. and Zou, M., Biosynthesis of Silver Nanoparticles Using the Biofilm Supernatant of *Pseudomonas aeruginosa* PA75 and Evaluation of Their Antibacterial, Antibiofilm, and Antitumor Activities, *Int. J. Nanomed*., 2023(18), 2485-2502 (2023). https://doi.org/10.2147/IJN.S410